Supplemental Materials for

"Spurious Indo-Pacific Connections to Internal Atlantic Multidecadal Variability Introduced by the Global Temperature Residual Method"

Clara Deser* and Adam S. Phillips

National Center for Atmospheric Research, Boulder, CO

Submitted 23 July 2022; Revised 30 October 2022

Geophys. Res. Lett.

* Corresponding author: Clara Deser (cdeser@ucar.edu)

Contents: This document contains a list of references, 4 Tables (Tables S1-S4) and 15 Figures (Figs. S1 – S15).

References

Danabasoglu, G., S. G. Yeager, Y. -O. Kwon, J. J. Tribbia, A. S. Phillips, and J. W. Hurrell, 2012. Variability of the Atlantic Meridional Overturning Circulation in CCSM4. *J. Climate*, 25, 5153-5172, doi: 10.1175/JCLI-D-11-00463.1.

Delworth, T. L., Cooke, W. F., Adcroft, A., Bushuk, M., Chen, J.-H., Dunne, K. A., et al. (2020). SPEAR: The next generation GFDL modeling system for seasonal to multidecadal prediction and projection. *Journal of Advances in Modeling Earth Systems*, 12, e2019MS001895. https://doi.org/10.1029/2019MS001895.

Kay, J. E., C. Deser, A. Phillips, A. Mai, C. Hannay, G. Strand, J. Arblaster, S. Bates, G. Danabasoglu, J. Edwards, M. Holland, P. Kushner, J. -F. Lamarque, D. Lawrence, K. Lindsay, A. Middleton, E. Munoz, R. Neale, K. Oleson, L. Polvani, and M. Vertenstein, 2015: The Community Earth System Model (CESM) Large Ensemble Project: A community resource for studying climate change in the presence of internal climate variability. *Bull. Amer. Met. Soc.*, 96, 1333–1349, doi: 10.1175/BAMS-D-13-00255.1.

Kirchmeier-Young, M. C., Zwiers, F. W. and Gillett, N. P. , 2017: Attribution of extreme events in Arctic Sea ice extent. J. Climate 30, 553–571.

Maher, N., Milinski, S., Suarez-Gutierrez, L., Botzet, M., Dobrynin, M., Kornblueh, L., et al. (2019). The Max Planck Institute Grand Ensemble: Enabling the exploration of climate system variability. *J. Adv. Mod. Earth Sys.*, 11, 2050– 2069. https://doi.org/10.1029/2019MS001639

Rodgers, K. B., Lee, S.-S., Rosenbloom, N., Timmermann, A., Danabasoglu, G., Deser, C., Edwards, J., Kim, J.-E., Simpson, I., Stein, K., Stuecker, M. F., Yamaguchi, R., Bodai, T., Chung, E.-S., Huang, L., Kim, W., Lamarque, J.-F., Lombardozzi, D., Wieder, W. R., and Yeager, S. G., 2021: Ubiquity of human-induced changes in climate variability, *Earth Syst. Dynam*, https://doi.org/10.5194/esd-2021-50, 2021.

Swart, N. C., Cole, J. N. S., Kharin, V. V., Lazare, M., Scinocca, J. F., Gillett, N. P., Anstey, J., Arora, V., Christian, J. R., Hanna, S., Jiao, Y., Lee, W. G., Majaess, F., Saenko, O. A., Seiler, C., Seinen, C., Shao, A., Sigmond, M., Solheim, L., von Salzen, K., Yang, D., and Winter, B.: The Canadian Earth System Model version 5 (CanESM5.0.3), *Geosci. Model Dev*., 12, 4823– 137 4873, https://doi.org/10.5194/gmd-12-4823-2019, 2019.

Tatebe, H., Ogura, T., Nitta, T., Komuro, Y., Ogochi, K., Takemura, T., Sudo, K., Sekiguchi, M., Abe, M., Saito, F., Chikira, M., Watanabe, S., Mori, M., Hirota, N., Kawatani, Y., Mochizuki, T., Yoshimura, K., Takata, K., O'Ishi, R., ... Kimoto, M. (2019). Description and basic evaluation of simulated mean state, internal variability, and climate sensitivity in MIROC6. *Geoscientific Model Development*, 12(7), 2727-2765. https://doi.org/10.5194/gmd-12-2727-2019.

Table S1. Model Large Ensembles used in this study.

Modeling Center	Model Version	Model Resolution (atm/ocn)	Years	Number of Members	Forcing	Reference
CCCma	CanESM2	~2.8°x2.8°/ ~1.4°x0.9°	1950-2100	50	historical, rcp85	Kirchmeier -Young et al. (2017)
MPI	MPI-ESM-LR	~1.9°x1.9°/ nominal 1.5°	1850-2100	100	historical, rcp85	Maher et al. (2019)
NCAR	CESM1-CAM5	~1.3°x0.9°/ nominal 1.0°	1920-2100	40	historical, rcp85	Kay et al. (2015)
CCCma	CanESM5	~2.8°x2.8°/ ~1.4°x0.9°	1850-2100	50	historical, ssp5-8.5	Swart et al. (2019)
GFDL	SPEAR_MED	50km/ nominal 1°	1921-2100	30	historical, ssp5-8.5	Delworth et al. (2020)
MIROC	MIROC6	~1.4°x1.4°/ nominal 1°	1850-2014	50	historical, ssp5-8.5	Tatebe et al. (2019)
NCAR	CESM2	~1.3°x0.9°/ nominal 1.0°	1850-2100	100	historical, ssp3-7.0	Rodgers et al. (2021)

Table S2. Observational data sets used in this study.

Name	**Acronym**	**Variable**	**Spatial Resolution**	**Years**
NOAA Extended Reconstruction SSTs Version 5	ERSSTv5	SST	2°x2°	1854-2022
Global Precipitation Climatology Centre	GPCC	PR	1°x1°	1891-2022
ECMWF Reanalysis 5th Generation	ERA5	PSL	0.25° x 0.25°	1950-2022

Table S3. Glossary of selected acronyms used in this study.

Acronym	Meaning
iAMV	Internal component of AMV
G, iG, fG	Total, internal and forced components of global-mean SST
SST, iPSL, iPR	Internal component of SST, PSL and PR obtained by removing the ensemble-mean component
iSST, iPSL, iPR	Internal component of SST, PSL and PR obtained by removing the ensemble-mean component
gresSST, gresPSL, gresPR	SST, PSL and PR after removing component associated with G
fgresSST, fgresPSL, fgresPR	SST, PSL and PR after removing component associated with fG
NA, iNA	Total and internal components of North Atlantic SST
gresNA, fgresNA	NA after removing the component associated with G, fG
iG_{NA}; iG*	Component of iG congruent with iNA; $iG\text{-}iG_{NA}$
$iAMVtruth_{NA}$	Regression maps of iSST, iPSL and iPR onto iNA
$iAMVtruth_{NA\text{-}G}$	Regression maps of iSST, iPSL and iPR onto iNA-iG
[$iAMVtruth_{NA}$], [$iAMVtruth_{NA\text{-}G}$]	Ensemble-means of $iAMVtruth_{NA}$, $iAMVtruth_{NA\text{-}G}$
iAMVgres	Regression maps of gresSST, gresPSL and gresPR onto gresNA
iAMVfgres	Regression maps of fgresSST, fgresPSL and fgresPR onto fgresNA
[iAMVgres], [iAMVfgres]	Ensemble-means of iAMVgres, iAMVfgres
MMLE	Multi-model Large Ensemble
SST_Obs, G_Obs	Observed SST, Observed global-mean SST
gresSST_Obs	SST_Obs after removing component associated with G_Obs
fgresSST_Obs	SST_Obs after removing component associated with models' fG
NA_Obs	Observed NA SST
NAgres_Obs, NAfgres_Obs	NA_Obs after removing component associated with G_Obs, models' fG
iAMVgres_Obs	Regression map of gresSST_Obs onto gresNA_Obs
iAMVfgres_Obs	Regression map of fgresSST_Obs onto fgresNA_Obs

Table S4. Global pattern correlations between: (a) [iAMVgres] and [$\text{iAMVtruth}_{NA\text{-}G}$]; (b) [iAMVfgres] and[$\text{iAMVtruth}_{NA}$]; and (c) ([iAMVgres] *minus* [iAMVfgres]) and ([$\text{iAMVtruth}_{NA\text{-}G}$] *minus* [$\text{iAMVtruth}_{NA}$]) for each model LE and the MMLE. Numbers to the left and right of the forward slash are based on the period 1950-2020 and 2030-2100, respectively. See main text for details and Table S3 for a glossary of terms.

		MPI	CESM1	CanESM2	MIROC6	CanESM5	SPEAR	CESM2	MMLE
(a)	SST	1.0/1.0	.95/.89	.93/.99	.97/.97	.91/.85	.96/.88	.95/.93	.97/.98
	PSL	1.0/1.0	.96/.93	.96/.99	.99/.99	.90/.86	.94/.93	.95/.93	.98/.99
	PR	1.0/1.0	.95/.86	.92/.99	.99/.98	.88/.85	.96/.94	.94/.92	.97/.98
(b)	SST	1.0/.99	.94/.94	.94/.99	.98/.97	.92/.89	.98/.85	.97/.91	.98/.98
	PSL	.99/.99	.95/.97	.95/.99	.97/.99	.85/.88	.89/.90	.98/.93	.98/.99
	PR	.99/.99	.94/.94	.95/.99	.97/.97	.85/.80	.92/.84	.97/.88	.96/.96
(c)	SST	1.0/1.0	.99/1.0	.98/.99	.99/.99	.98/.98	.97/.99	.99/.99	.99/1.0
	PSL	1.0/1.0	.99/.99	.99/1.0	1.0/1.0	1.0/.99	.98/.99	.99/1.0	1.0/1.0
	PR	1.0/1.0	1.0/.99	1.0/1.0	1.0/1.0	1.0/.99	.99/.99	1.0/1.0	1.0/1.0

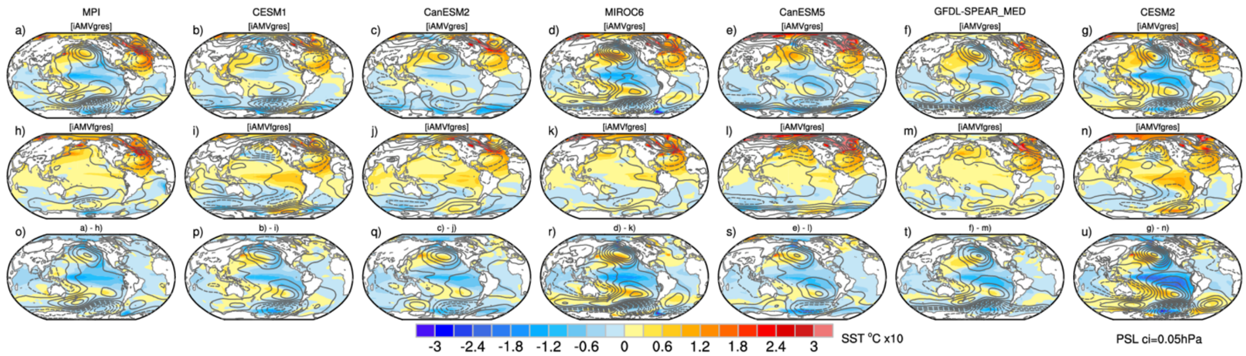

Figure S1. Ensemble-mean iAMV regression maps for SST (color shading) and PSL (contours; negative values dashed) based on 1950-2020 for each model Large Ensemble using the following methods: (top row) [iAMVgres]; (middle row) [iAMVfgres]; and (bottom row) top minus middle. See main text for explanation.

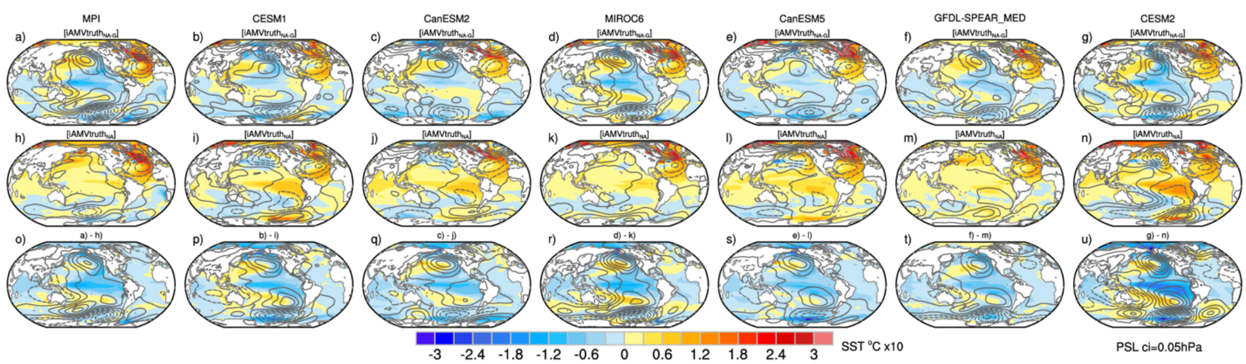

Figure S2. Ensemble-mean iAMV regression maps for SST (color shading) and PSL (contours; negative values dashed) based on 1950-2020 for each model Large Ensemble using the following methods: (top row) [iAMVtruth$_{NA-G}$]; (middle row) [iAMVtruth$_{NA}$]; and (bottom row) top minus middle. See main text for explanation.

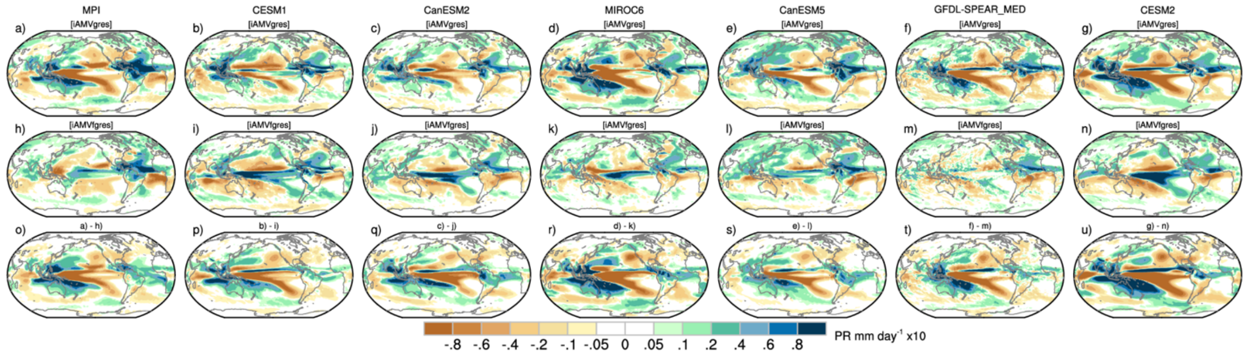

Figure S3. As in Fig. S1 but for PR.

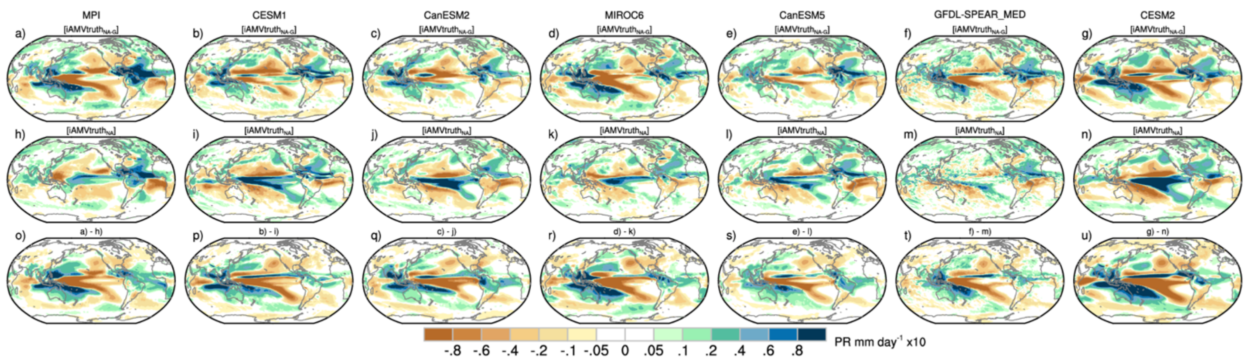

Figure S4. As in Fig. S2 but for PR.

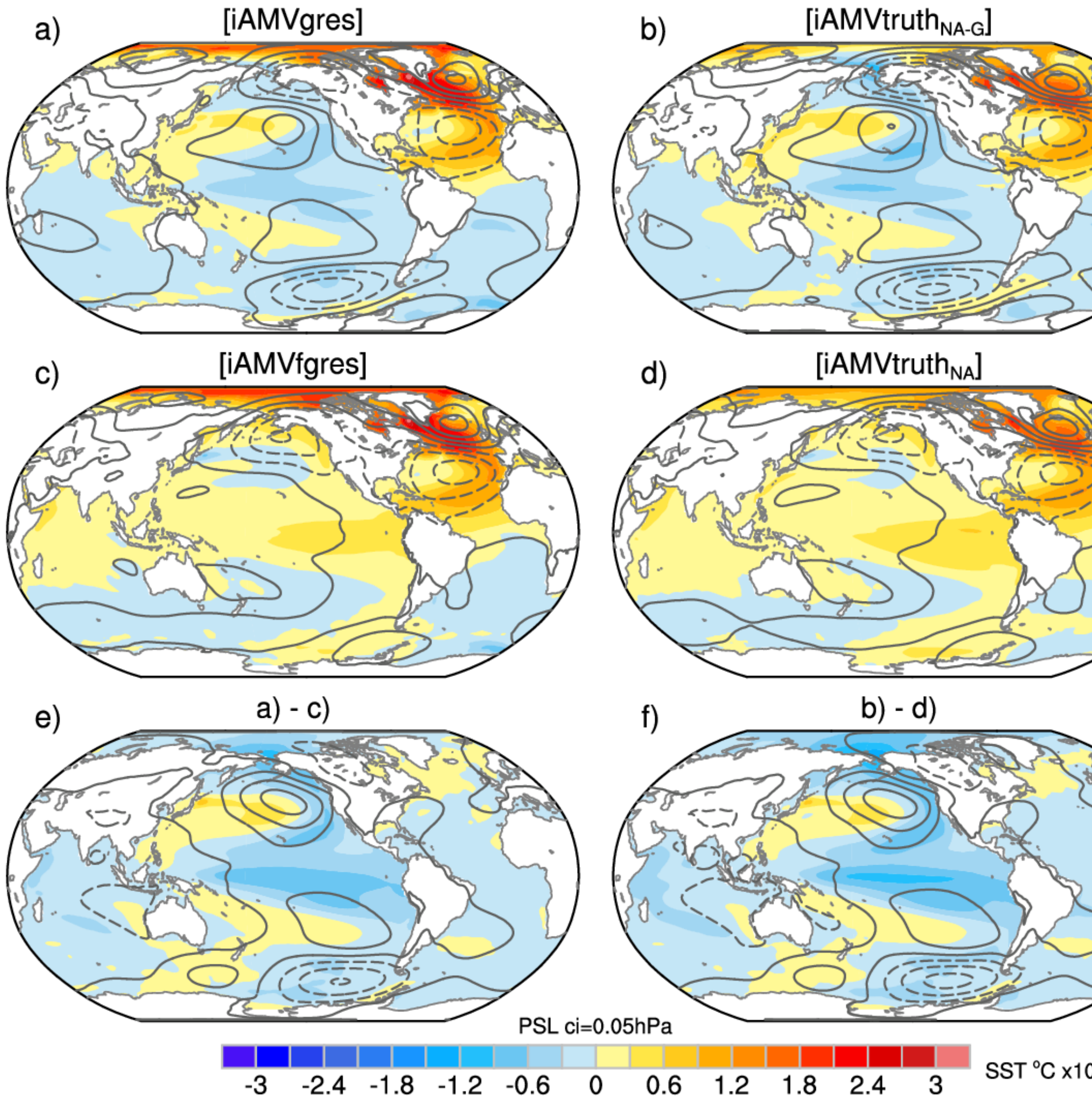

Figure S5. Multi-Model Large Ensemble iAMV regression maps for SST (color shading) and PSL (contours; negative values dashed) based on 2030-2100 using the following methods: (a) [iAMVgres]; (b) [iAMVtruth$_{NA-G}$]; (c) [iAMVfgres]; (d) [iAMVtruth$_{NA}$]; (e) a-c; f) b-d. See main text for explanation.

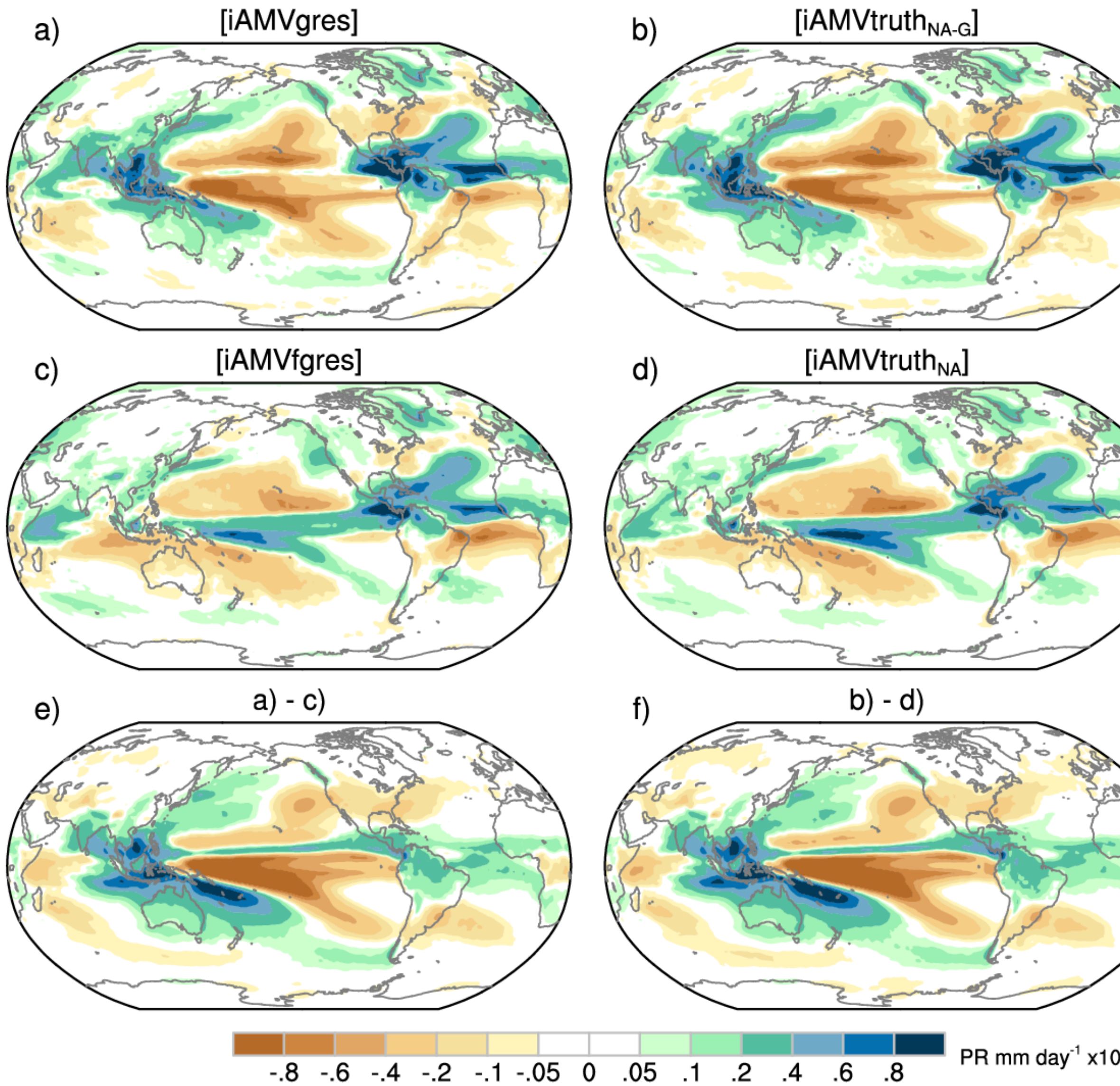

Figure S6. As in Fig. S5 but for PR.

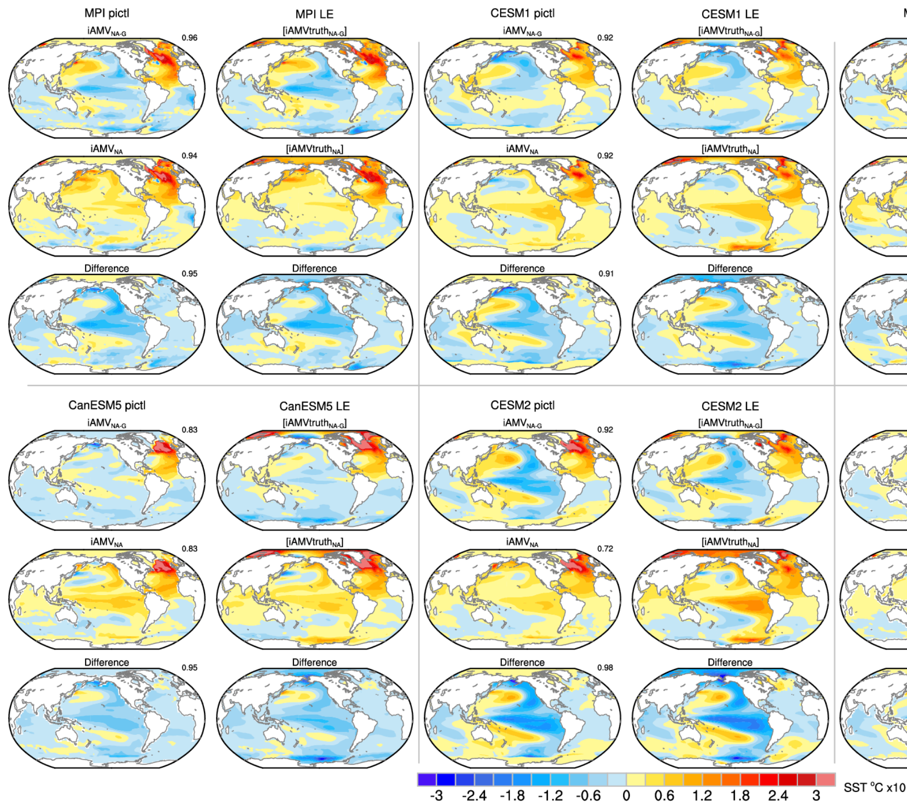

Figure S7. Comparison of iAMV SST regression maps from (left) preindustrial control (pictl) and (right) historical (1950-2020) Large Ensemble simulations for MPI, CESM1, MIROC6, CanESM5 and CESM2 (pictl simulations are not available for CanESM2 and GFDL-SPEAR_MED). The MME panel shows the average of the regression maps across the 5 models. For the pictl simulations, the top and middle panels show regressions onto the NA-G and NA SST indices (denoted $iAMV_{NA-G}$ and $iAMV_{NA-G}$, respectively); the bottom panel shows the difference between the top and middle panels. For the LE simulations, the top and middle panels show [$iAMVtruth_{NA-G}$] and [$iAMVtruth_{NA}$], respectively, and the bottom panel shows the difference between the top and middle panels. SSTs from the pictl simulations were detrended and low-pass filtered using a 10-yr Butterworth filter. The length of the pictl simulations are as follows: MPI (2001 years); CESM1 (1800 years); MIROC6 (800 years); CanESM5 (1000 years); and CESM2 (1900 years). The numbers in the upper right of the pictl panels indicate the global (60ºN-60ºS) spatial correlation with the adjacent Truth panel. For example, the spatial correlation between $iAMV_{NA-G}$ and [$iAMVtruth_{NA-G}$] is 0.96 for MPI and 0.98 for MME.

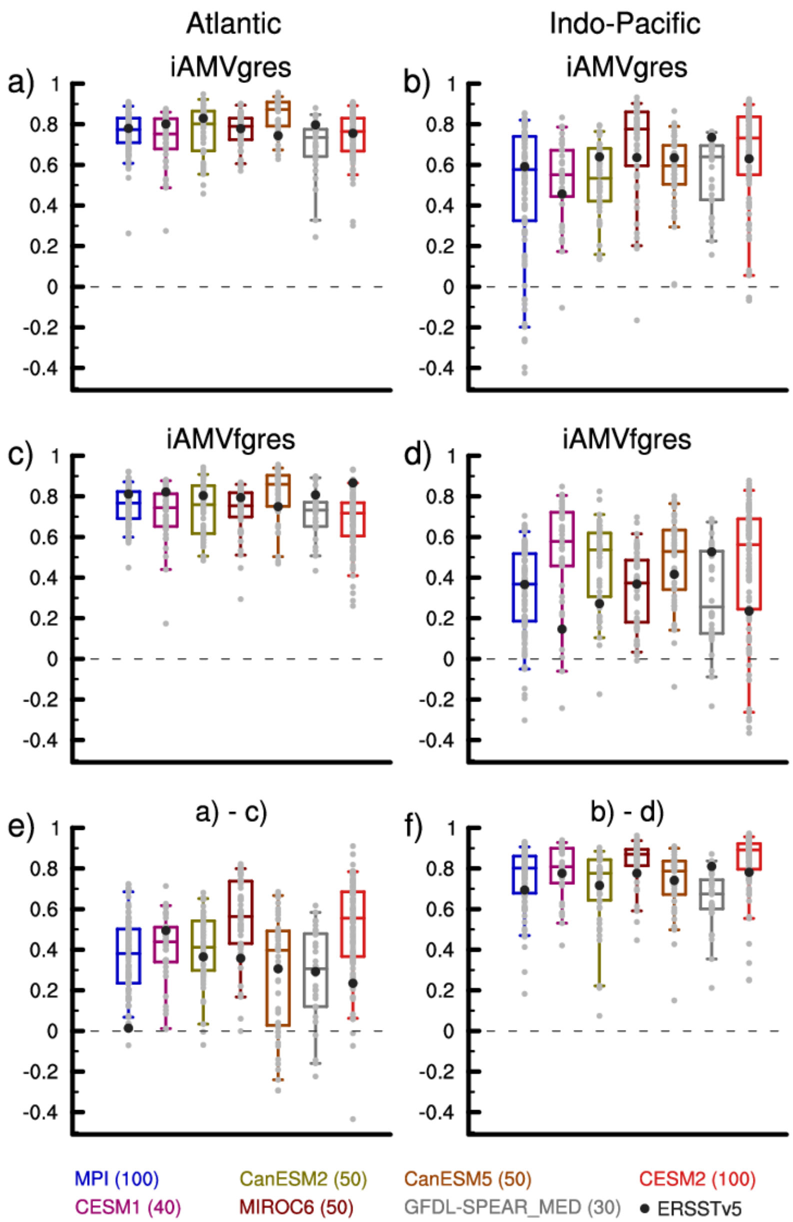

Figure S8. Distribution of iAMV SST pattern correlations between each ensemble member and the ensemble-mean (gray dots) for each model LE based on 1950-2020 using the following methods: (a,b) iAMVgres; (c,d) iAMVfgres; and (e,f) iAMVgres minus iAMVfgres. Boxes outline the 25th-to-75th percentile range, and whiskers show the 5th-to-95th percentile range. Black dots indicate correlations between observations and the model ensemble-means. Left column (a,c,e): Atlantic (80°W-30°E); Right column (b,d,f): Indo-Pacific (defined as the region outside the Atlantic).

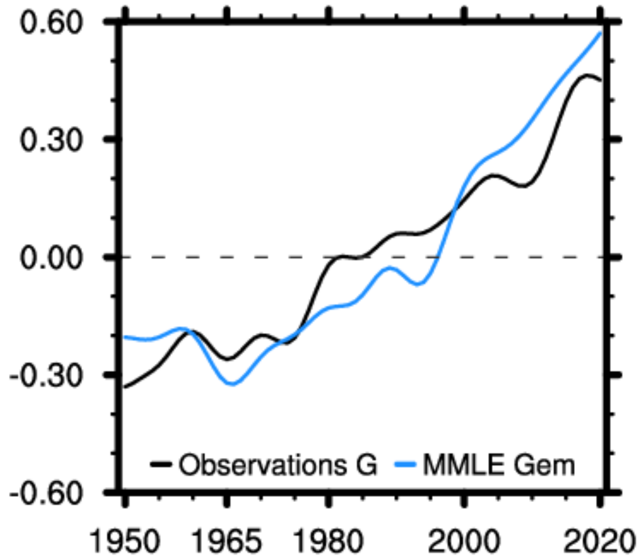

Figure S9. Global-mean (60ºN-60ºS) low-pass filtered SST anomaly timeseries (ºC) based on observations (black curve) and the MMLE ensemble-mean (blue curve).

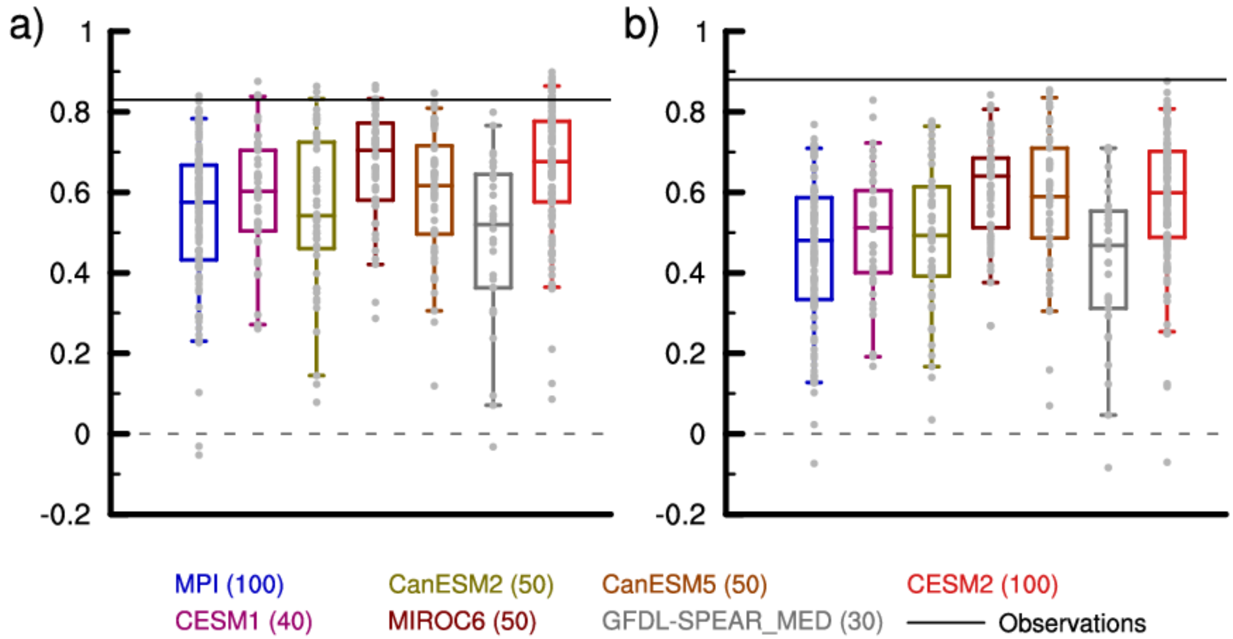

Figure S10. Distribution of temporal correlations between IPV and the difference between the gresNA and fgresNA SST indices for each ensemble member of each model LE based on 1950-2020 (gray dots) at (a) zero-lag and (b) IPV leading by 1 yr. Boxes outline the 25th-to-75th percentile range, and whiskers show the 5th-to-95th percentile range. The horizontal black line indicates the observed correlation value.

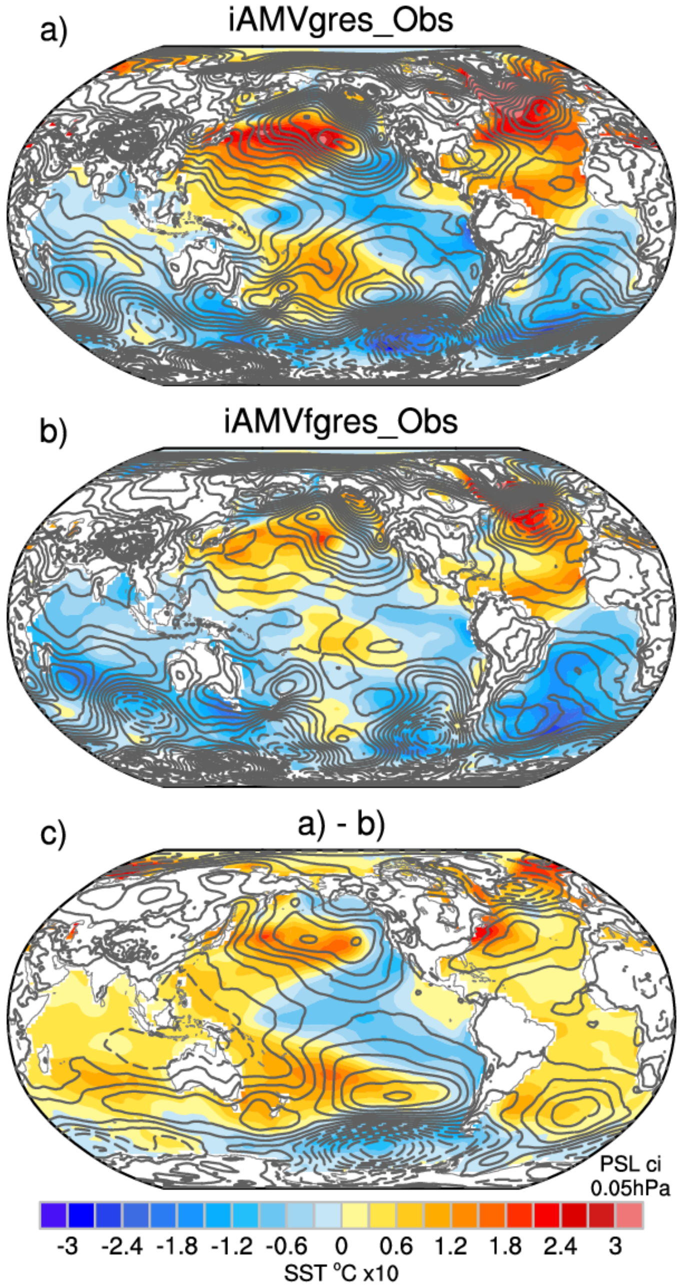

Figure S11. Observed iAMV regression maps for SST (color shading) and PSL (contours; negative values dashed) based on 1950-2020 using the following methods: (a) iAMVgres; (b) iAMVfgres; and (c) iAMVgres minus iAMVfgres. See main text for explanation.

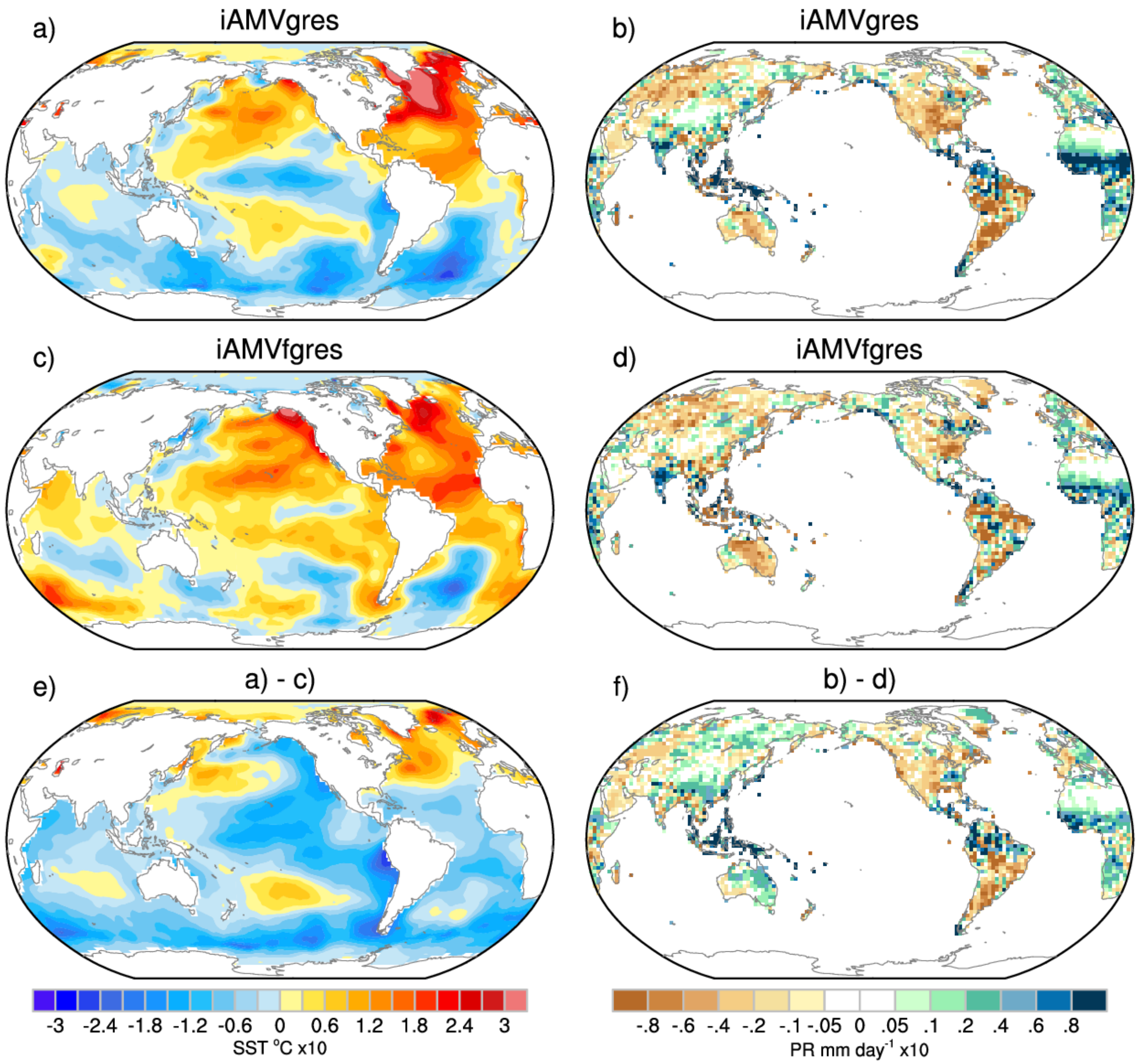

Figure S12. Observed iAMV SST (left) and PR (right) regression maps based on 1900-2020 using the following methods: (a,b) iAMVgres; (c,d) iAMVfgres; and (e,f) iAMVgres minus iAMVfgres. See main text for explanation.

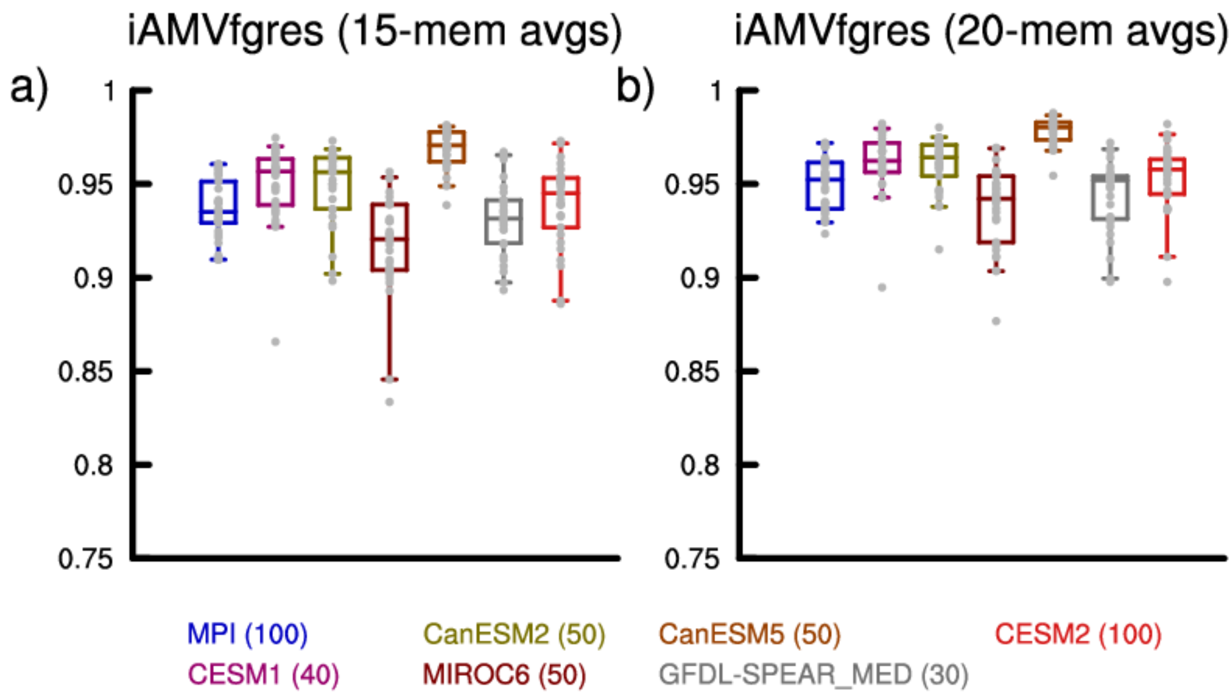

Figure S13. Sampling variability of [iAMVfgres] SST regression patterns based on (a) 15-member averages and (b) 20-member averages for the period 1950-2020. For each model LE, we construct 15-member and 20-member averages of the SST iAMV patterns obtained with the fG-Res method by randomly selecting (with replacement) from the full set of members. We repeat this procedure 30 times for each model LE, and then compute the global pattern correlations between the full-member average and each of the thirty 15-member and 20-member averages for each model LE (gray dots). Boxes outline the 25th-to-75th percentile range, and whiskers show the 5th-to-95th percentile range.

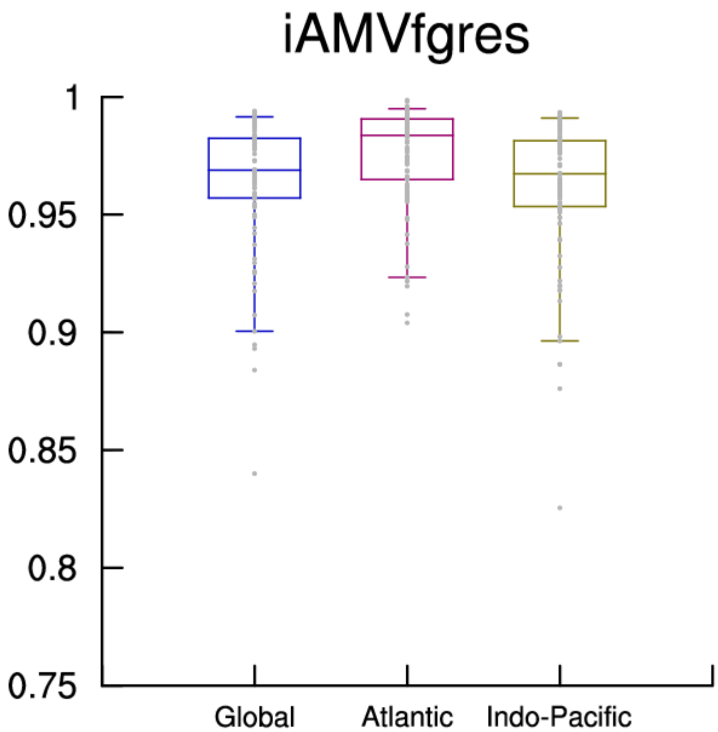

Figure S14. Sampling variability of iAMVfgres_Obs SST regression pattern for the period 1950-2020. We compute 6-member averages of G(t) by randomly sampling (with replacement) from the full set of 420 simulations across the 7 model LEs, and repeat this procedure 100 times. We compute pattern correlations between iAMVfgres_Obs based on the full 420-member average to define fG(t) with that based on each of the 100 6-member averages to define fG(t) (gray dots) for the global, Atlantic and Indo-Pacific domains. Boxes outline the 25th-to-75th percentile range, and whiskers show the 5th-to-95th percentile range.

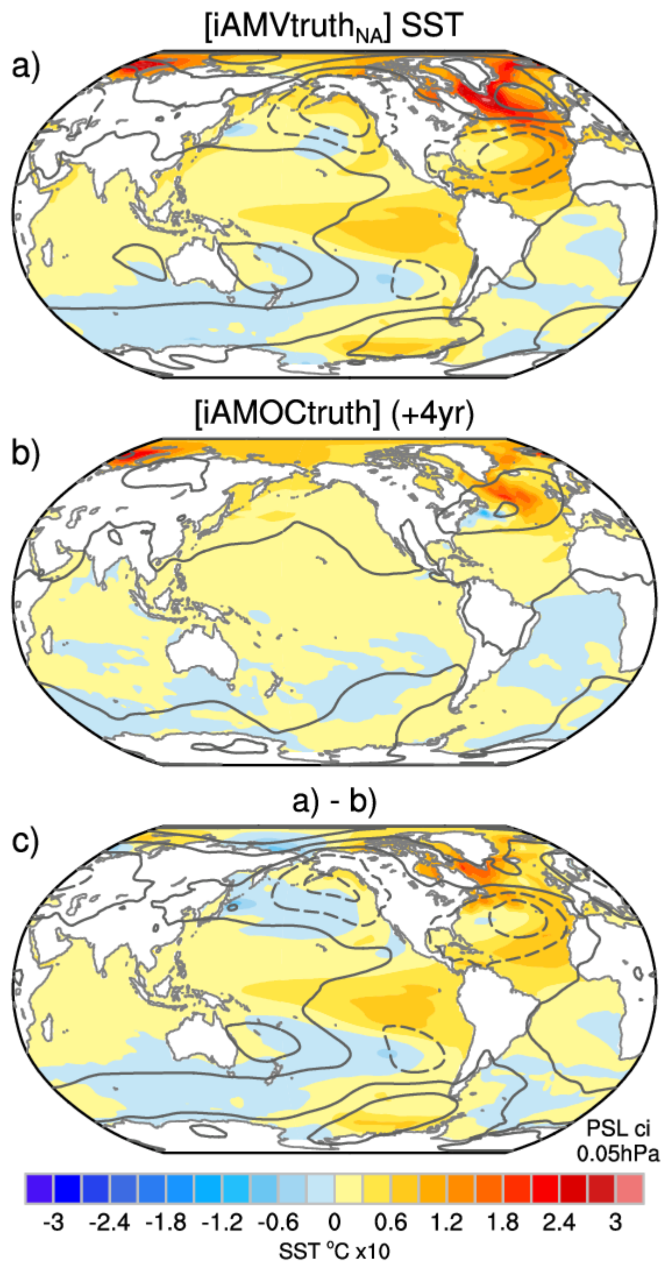

Figure S15. Multi-Model Large Ensemble ensemble-mean regression maps for SST (color shading) and PSL (contours; negative values dashed) based on 1950-2020 using the Truth method and the following normalized indices: (a) North Atlantic (NA) SST; (b) Atlantic Meridional Overturning Circulation (AMOC) leading by 4 years, where AMOC is defined as the leading principal component timeseries of oceanic meridional mass transport in the Atlantic sector between 33°S-90°N following Danabasoglu et al. (2012); and (c) their difference. See main text for explanation. The MIROC6 LE is excluded from all calculations due to lack of AMOC data.